Identification of intraneuronal amyloid beta oligomers in locus coeruleus neurons of Alzheimer's patients and their potential impact on inhibitory neurotransmitter receptors and neuronal excitability

Kelly, Louise; Seifi, Mohsen; Ma, Ruolin; Mitchell, Scott J.; Rudolph, Uwe; Viola, Kirsten L.

Published in:
Neuropathology and Applied Neurobiology

DOI:
10.1111/nan.12674

Publication date:
2020

Document Version
Peer reviewed version

PROFESSOR JEROME D SWINNY (Orcid ID : 0000-0002-8194-5481)

Article type : Original Article

Title

Identification of intraneuronal amyloid beta oligomers in locus coeruleus neurons of Alzheimer's patients and their potential impact on inhibitory neurotransmitter receptors and neuronal excitability.

Running title

Amyloid beta oligomers in the locus coeruleus in Alzheimer's

Authors and affiliations

Louise Kelly [1*], Mohsen Seifi [1,2], Ruolin Ma [1], Scott J Mitchell [3**], Uwe Rudolph [4], Kirsten L. Viola [5], William L. Klein [5], Jeremy J. Lambert [2], Jerome D. Swinny [1***]

[1] School of Pharmacy & Biomedical Sciences, University of Portsmouth, Portsmouth, PO12DT, United Kingdom

[2] Leicester School of Pharmacy, De Montfort University, Leicester, LE1 9BH, United Kingdom

[3] Neuroscience, Division of Systems Medicine, Ninewells Hospital & Medical School, Dundee University, Dundee, DD19SY, Scotland, United Kingdom

[4] Department of Comparative Biosciences, College of Veterinary Medicine, and Carl R. Woese Institute for Genomic Biology, University of Illinois at Urbana-Champaign, Urbana, IL, USA

[5] Department of Neurobiology and Physiology, Northwestern University, Evanston, Illinois, USA

* Current address: Faculty of Medicine, University of Southampton, Southampton, UK
** Current address: UK Dementia Research Institute at Kings College London, London, UK.
***** Corresponding author**
Professor Jerome Swinny, School of Pharmacy and Biomedical Sciences, University of Portsmouth, St Michael's Building, White Swan Road, Portsmouth, PO12DT, UK
Tel: +44 (0) 2392842076
Email: jerome.swinny@port.ac.uk

Data availability

The data that support the findings of this study are openly available in the University of Portsmouth Research Portal (Pure): https://researchportal.port.ac.uk/portal/en/

Abstract

Aims

Amyloid β oligomers (AβO) are potent modulators of Alzheimer's pathology, yet their impact on one of the earliest brain regions to exhibit signs of the condition, the locus coeruleus (LC), remains to be determined. Of particular importance is whether AβO impact the spontaneous excitability of LC neurons. This parameter determines brain-wide noradrenaline (NA) release, and thus NA-mediated brain functions, including cognition, emotion and immune function, which are all compromised in Alzheimer's. Therefore, the aim of the study was to determine the expression profile of AβO in the LC of Alzheimer's patients and to probe their potential impact on the molecular and functional correlates of LC excitability, using a mouse model of increased Aβ production (APP-PSEN1).

Methods and Results

Immunohistochemistry and confocal microscopy, using AβO-specific antibodies, confirmed LC AβO expression both intraneuronally and extracellularly in both Alzheimer's and APP-PSEN1 samples. Patch clamp electrophysiology recordings revealed that APP-PSEN1 LC neuronal hyperexcitability accompanied this AβO expression profile, arising from a diminished inhibitory effect of GABA, due to impaired expression and function of the GABA-A receptor ($GABA_AR$) α3 subunit. This altered LC α3-$GABA_AR$ expression profile overlapped with AβO expression in samples from both APP-PSEN1 mice and Alzheimer's patients. Finally, strychnine-sensitive glycine receptors (GlyRs) remained resilient to Aβ-induced changes and their activation reversed LC hyperexcitability.

Conclusions

The data suggest a close association between AβO and α3-$GABA_ARs$ in the LC of Alzheimer's patients, and their potential to dysregulate LC activity, thereby contributing to the spectrum of pathology of the LC-NA system in this condition.

Introduction

Synaptic dysfunction is a key pathological mechanism underlying the mild cognitive, memory and neuropsychiatric impairments that typify the earliest stages of Alzheimer's [1-3]. Given the brain's established propensity for synaptic remodelling, identifying the molecular and cellular mechanisms of such synaptic pathology, prior to the onset of irreversible neuronal death, likely represents one of the best interventional strategies against this disease [4, 5]. Convergent lines of evidence point to a crucial role for the soluble, oligomeric variants of amyloid β (AβO) [6, 7] in mediating such synaptic dysregulation [8, 9].

Experimentally, AβO bind directly to synaptic junctions [9-11], alters excitatory and inhibitory synaptic transmission [12-14], the expression and location of synaptic neurotransmitter receptors [15, 16] as well influencing synaptic plasticity [14] and learning and memory [17]. This association is also evident in humans, with a strong association demonstrated between AβO and dementia [18, 19]. While such compelling evidence exist for AβO pathology in cortical brain regions, less is known about the impact of this pathway in one of the first regions to exhibit quintessential Alzheimer's histopathology, namely the locus coeruleus (LC) [20, 21]. In particular, we do not know whether AβO-related pathology alters the core determinant of LC-mediated brain functions, the spontaneous neuronal firing rate, and if so, through which mechanisms?

The relevance of LC neurobiology to the understanding of the spectrum Alzheimer's-related symptoms is underscored by the overlap between the brain functions, this system modulates, and those that are impaired in this condition. These include cognition [22], arousal [23], emotion [24] and the stress response [25]. The coordinated brain-wide release of the LC's signature neurotransmitter noradrenaline (NA), and thus LC-NA mediated brain functions, arises from the complex firing patterns of LC neurons, which are brain [26], behaviour [23, 27] and disease-state [28] dependent. This emphasises the importance of understanding the molecular machinery of the LC and how this contributes to regulating LC neuronal excitability in health and disease [29].

The focus on Alzheimer's pathology within the LC has been predominantly on hyperphosphorylated tau tangles [21] because of their early presence during the disease spectrum. Despite confirmation of the native expression of LC intraneuronal Aβ peptides in rodents at least [30, 31], Aβ-related pathology has largely been overlooked because only insoluble Aβ-containing plaques have been documented within the LC, and they are present only in the final stages of the condition [32]. Therefore, neither the presence of the more toxic soluble AβO within LC, nor their effects on LC neuronal excitability, have been demonstrated. This is important because of the evidence indicating that AβO, rather than Aβ plaques, mediate the neuro-toxic effects of the Aβ pathway [33, 34]. Of particular relevance to the LC, and its early involvement in Alzheimer's pathology, is the emerging synergistic role of AβO in tau tangle formation [35, 36]. Intriguingly, while notable LC neuronal loss, attributed to tauopathy, is a core feature in Alzheimer's [37], there appears to be discordance between the onset of such pathology, and LC neurodegeneration [20]. Given such considerable evidence, it is reasonable to speculate that in the LC, initial, pre-symptomatic insults in the form of tau tangle and AβO interactions, cooperate to set in motion a range of pathological changes such as synaptic dysfunction, oxidative stress [38] and altered LC excitability [28]. Such changes are likely to prove crucial in terms of the long-term viability of cells not only within the LC, but also in other brain regions because impaired LC integrity directly influences the progression of Alzheimer's pathology in cortical regions [39, 40]. To begin to explore the potential influence of AβO on the LC-NA system, and thus connected brain regions, we investigated the impact of Aβ, and AβO in particular, on the molecular and physiological correlates of the LC.

Materials and Methods

See the Supplementary Information (SI) section for detailed descriptions of methodology.

Animals

The B6C3-Tg (APPswe, PSEN1dE9) double transgenic mouse model, that results in accelerated production of Aβ [41], (APP-PSEN1), bred on a C57BL/6J background strain, 2 and 4 months of age, was the main strain used in the study. In all experiments, wild type (WT) littermates were used as controls for APP-PSEN1 subjects. In a subset of experiments, $GABA_AR$ α3 subunit gene deleted ($\alpha3^{-/-}$) mice and their WT littermates [42], bred on a C57BL/6J background, as well as mice expressing green fluorescent protein (GFP) under the promotors of the astroglial cytoskeletal protein, glial fibrillary acidic protein (GFP-GFAP) [43] were used. Male mice were used throughout all experiments.

Human tissue

Formalin-fixed, paraffin embedded, 8 μm thickness brain sections containing the LC were provided by Brains for Dementia Research tissue banks, from n = 5 control and 5 Alzheimer's subjects. Demographic details of the subjects are detailed in SI Table 1.

Immunohistochemistry and confocal microscopy

Experiments were conducted according to previously described protocols [44]. Briefly, mice were transcardially perfusion fixed with 1% paraformaldehyde. The brains were sectioned using a vibratome and tissue sections incubated using a range of primary and secondary antibodies (see SI Table 2 for details of primary antibodies used). Sections were examined with a confocal laser-scanning microscope (LSM710 or LSM880; Zeiss, Germany), images were processed using Zen 2009 Light Edition (Zeiss) and figures prepared using Adobe Photoshop. For semi-quantitative analyses, see additional details in SI section.

Whole-cell patch clamp electrophysiology LC recordings in acute brain slices of AP-PSEN1 and WT

Spontaneous LC firing rate (FR), in the absence or presence of a range of neurotransmitter modulators, was determined in 2-4 month-old mice, according to previously published protocols [45, 46].

Quantitative reverse transcription polymerase chain reaction (qPCR)

Changes in the mRNA levels for the following inflammatory genes were quantified in samples from the LC and hippocampus, according to our previously published protocols [47]: IL1β, IL6, CSF1, CLC2/3; IBA1, TNFα (see SI for primer details).

Enzyme-linked immunosorbent assay (ELISA)

An ELISA was used to measure the concentration of NA (catalogue number BA E-5200, LDN, Germany) in blood and brain respectively, according to manufacturer's protocols

Statistical analysis

The individual statistical tests used to assess specific data sets are indicated in the Results section. An alpha-level of less than 0.05 that was used to determine statistical significance. For graphical presentation of quantitative data, symbols represent individual data points, bars represent the means and the error bars the SEM. In all cases, GraphPad Prism was used for statistical analyses and graphical presentation of the data.

Results

Expression of AβO within the LC of Alzheimer's patients and APP-PSEN1 mice

While plaques composed of fibrillar Aβ have been reported in the LC of Alzheimer's patients, localisation of oligomers in this brain region remain to be demonstrated. Immunoreactivity for an antibody (4G8), which recognises both fibrillar and oligomeric forms of Aβ, presented predominantly as extracellular plaques within the LC of post-mortem samples from Alzheimer patients. There was minimal apparent association with noradrenergic profiles (Fig. 1 A1). This is in agreement with previously published reports [32]. No specific signal was detected in human control samples (SI Fig. 1 A). In comparison to Alzheimer's samples, Aβ immunoreactivity in the LC of APP-PSEN1 mice, using antibodies that recognise different sequences of the peptide (clones 4G8 and WO-2), invariably presented as cytoplasmic signal within TH-immunopositive neurons as well as TH-immunonegative cells [44] (Fig. 1 A2-4). This expression pattern is similar to previous reports of native LC Aβ expression in rodent [30, 31]. No specific signal was detected in WT samples (SI Fig. 1 B). The LC TH-immunonegative, Aβ-immunopositive cells were confirmed to be neurons, using the pan-neuronal marker HuC [48], (SI Fig. 2A). They were further distinguished by the expression of calretinin (SI Fig. 2B) or calbindin (SI Fig. 2C).

Even though native LC Aβ expression has been demonstrated in rodent in a manner similar to the cytoplasmic profile in Fig. 1 A2-4, an important caveat for the above data is that the 4G8 and WO-2 antibodies used in this study are capable of binding to APP in addition to Aβ. We therefore confirmed the expression of AβO, in LC neurons, using AβO-specific antibodies. Two different antibodies were used that have been demonstrated to specifically recognise human AβO in samples from Alzheimer's patients, and not control human subjects, here termed NU1 and NU2 [49]. Both antisera have been shown to exhibit strong binding to trimers, tetramers, and 12–24mer, but not monomers [49]. AβO-NU2, produced intense cytoplasmic staining of LC neurons in Alzheimer's samples, as well as numerous extracellular immunoreactive clusters (Fig. 1 B). No specific signal was detected in human control samples (SI Fig. 3 A), in agreement with previous evidence using cortical samples [49]. This suggests a novel significant interaction between LC neurons and the oligomeric forms of Aβ during the disease. An

overview of immunoreactivity for AβO-NU2 in the LC of APP-PSEN1 mice revealed a largely intraneuronal pattern that closely mirrored that found in Alzheimer's samples (Fig. 1 C1-2). Whilst the signal was distributed widely throughout the LC, it was noticeable that some TH-immunopositive cells were devoid of any AβO-NU2 immunoreactivity (Fig. 1 C3). Higher resolution inspection indicated that AβO-NU2 immunoreactivity was concentrated in TH-immunopositive somata, dendrites and fine processes suggestive of axons, and extracellular clusters (Fig. 1 C4). We used WT mouse samples to confirm the specificity of APP-PSEN1 AβO-NU2 signal since they lack human APP or Aβ (SI Fig. 3C). Immunoreactivity for AβO-NU1 in APP-PSEN1 mice closely resembled that of AβO-NU2. However, a notable difference was the significant variation in the intensity of signal between different LC TH-immunopositive neurons (Fig. 1 D), suggesting different expression levels across LC noradrenergic neurons. No specific AβO-NU1 signal was detected in WT mouse samples (SI Fig. 3B). Despite strong AβO-NU1 immunoreactivity being previously reported using human cortical samples [49], we were unable to detect any specific AβO-NU1 signal in the LC of patient samples (data not shown).

A proposed pathway for intraneuronal AβO in Alzheimer's pathogenesis is its incorporation into the mitochondrial matrix and disruption of cellular bioenergetics [50]. Immunoreactivity for citrate synthase, an enzyme located within the mitochondrial matrix [51], was used to explore the association between AβO-NU1/2 and mitochondrial compartments in APP-PSEN1 mice. There was a significant overlap between somatic immunoreactivity for AβO-NU1 (Fig. 1 E1-2) and AβO-NU2 (Fig. 1 F1-2) and the signal for citrate synthase. Quantification of the degree of colocalised pixels between citrate synthase:AβO-NU1 (Fig. 1 E3) and citrate synthase:AβO-NU2 (Fig. 1 F3) revealed positive correlations for both the degrees of co-occurrence of overlapping pixels, using the Manders' overlap coefficient [52], (NU1: median, range; 0.5, 0.1 - 0.9, n = 100 cells, Fig. 1 E3), (NU2: median, range: 0.6, 0.33-0.9, n = 100 cells, Fig. 1 F3) as well as the intensities of overlapping pixels, using the Pearson's correlation coefficient [53] (NU1: median, range; 0.4, 0.1 - 0.7, n = 100 cells, Fig. 1 E3), (NU2: median, range: 0.4, 0.2-0.8, n = 100 cells, Fig. 1 F3). There was also a striking overlap of citrate synthase-AβO-NU1/2 for immunoreactive clusters neighbouring the periphery of somata and dendrites, which could be indicative of the location of axonal terminals.

A consequence of AβO-mediated mitochondrial dysfunction is oxidative stress [38, 54] with mitochondrial oxidative stress associated with the FR and viability of LC neurons [28]. A key mitochondrial enzyme in this process is superoxide dismutase 2 (SOD2). It provides protection against AβO-mediated oxidative stress [55] and its expression is decreased in Alzheimer's [56]. We detected a positive association for the location of SOD2 immunoreactive clusters with both AβO-NU1 (Fig. 1 G) and AβO-NU2 (Fig. 1 H). In comparison to WT samples, there was a noticeable decrease in the intensity of SOD2 immunoreactivity in the LC of APP-PSEN1 mice (Fig. 1 I1-6), which was borne out by a quantitative assessment of the respective fluorescence intensities, in samples reacted and imaged under identical conditions (P = 0.02, two-tailed unpaired Student's t test; n = 5 animals) (Fig. 1 I7). This collectively suggests a strong association of intraneuronal AβO with mitochondrial compartments of LC neurons.

Neuroinflammation is a core component of Alzheimer's pathology with both Aβ fibrils [57] and AβO mediating specific pathways [58]. A distinctive feature of Alzheimer's related neuroinflammation is the presence of activated microglia. We therefore assessed the LC of APP-PSEN1 mice for signs of altered immune status, using the microglia/macrophage-specific calcium-binding protein ionized calcium binding adaptor molecule 1 (IBA1), the expression of which is increased in Alzheimer's-associated neuroinflammation [57]. TH-immunopositive neurons in the LC of APP-PSEN1 mice appeared to be contacted by a greater number of IBA1-immunoreactive profiles which were also more ramified, compared to WT, suggesting increased expression levels of this inflammatory marker (Fig. 1 J1-2). This increased expression was confirmed at both mRNA (P = 0.0053, two-tailed unpaired Student's t test; n = 10 animals) (Fig. 1 J3) and cell density levels (P <0.0001, two-tailed unpaired Student's t test; n = 10 animals) (Fig. 1 J4). The production of inflammatory cytokines is considered to be a consequence of microglial activation in Alzheimer's [57]. Since the LC of APP-PSEN1 mice exhibits only the oligomeric forms of Aβ, whilst oligomeric as well as fibrillar expression is evident in cortical regions, we assessed whether there were differences in the levels of inflammatory cytokines between the LC and hippocampus. Accordingly, we detected contrasting cytokine expression profiles in the LC and hippocampus. mRNA expression for colony stimulating factor 1

receptor (CSF1), which is anti-inflammatory and prevents the progression of Alzheimer's-like pathology [59], was significantly decreased in the LC (P = 0.0013, 2-ANOVA, Sidak's; n = 5 animals), yet upregulated in the hippocampus (P = 0.0045, 2-ANOVA, Sidak's; n = 5 animals) (Fig. 1 J5). Since CSF1 signalling purportedly promotes neuroprotection [60], its contrasting expression profiles in the LC and hippocampus, as a result of Alzheimer's-like pathology, could be a contributing factor to the early vulnerability of the LC to Alzheimer's. In contrast, whilst the mRNA levels for interleukin 1 beta (IL-1β) (P= 0.0081, two-way ANOVA with Sidak's; n = 5 animals) (Fig. 1 J6) and chemokine (C-C motif) ligand 3 (CCL3) (P = 0.0216, 2-ANOVA, Sidak's; n = 5 animals) (Fig. 1 J7) were significantly increased in hippocampal samples, no significant changes were detected in the LC.

AβO are associated with LC synapses and LC neuronal hyperexcitability in APP-PSEN1 mice

Apart from the cytoplasmic expression profile of AβO-NU1-2 outlined above, numerous extracellular immunoreactive clusters that decorated LC neuronal surfaces were also evident. Since AβO have been shown to interact at synaptic domains [49], we next assessed the association of AβO immunoreactivity with signal for synaptic marker proteins. In APP-PSEN1 mice, clusters immunoreactive for AβO-NU2 were located in close apposition to puncta immunopositive for the synaptic vesicle glycoprotein 2A (SV2A) (Fig. 2 A). This protein is expressed in excitatory and inhibitory synapses and is thus representative of the location of all synaptic junctions [61]. Furthermore, AβO-NU2 immunoreactivity was in close contact with clusters immunoreactive for the vesicular GABA transporter (VGAT), a marker of inhibitory synapses (Fig. 2 B) as well as the vesicular glutamate 2 (VGLUT2), a marker of excitatory synapses (Fig. 2 C).

Given the important role that synaptic transmission has in setting the spontaneous firing rate (FR) of LC neurons, and the established impact of AβO on synaptic transmission discussed previously, we next assessed the functional consequences of the increased AβO expression in APP-PSEN1 mice, by recording LC spontaneous FRs from identified NA LC neurons (Fig. 2 D). APP-PSEN1 LC neurons exhibited significantly greater FRs (P < 0.001; two-tailed unpaired Student's t test; n = 32 WT and 35 APP-PSEN1 cells) (Fig. 2

D2-3) and decreased membrane time constant compared to WT (P = 0.038, two-tailed unpaired Student's t test, n = 9 cells) (Fig. 2 D4). No other changes in LC physiological parameters were detected (Table 1). Accompanying this enhanced LC excitability was a significant decrease in NA concentration in the LC (P = 0.0032, 2-ANOVA, n =5 animal), and a significant increase in the hippocampal content (P < 0.0001, 2-ANOVA, n =5 animal) (Fig. 2 E).

In light of this heightened excitability of LC neurons, we next assessed whether this could be due to changes in inhibitory modulation. GABA and glycine provide the predominant inhibitory modulation of LC neurons [62]. We therefore explored whether the increased levels of AβO in AP-PSEN1 impacts on these pathways in regulating basal spontaneous FR. Using a recording electrode solution that is representative of the native intracellular Cl^- ion concentration, bath-applied GABA induced a concentration dependent decrease in the spontaneous FR of WT LC neurons with an approximate IC_{50} of 100 nM (Fig. 2 F1). With this concentration of GABA, there was a significant drug [$F_{(1, 18)}$ = 12.38, P = 0.0025, two-way ANOVA with repeated measures (2-RMA)] and genotype [$F_{(1, 18)}$ = 7.685, P = 0.0126, 2-RMA] effect on FR. However, *post-hoc* analysis revealed that while GABA (100 nM) significantly inhibited FR in WT cells (P = 0.0142, Sidak's; n = 7 cells), this effect was abolished in cells from APP-PSEN1 mice (P = 0.1665, Sidak's; n = 12 cells) (Fig. 2 F2). Calculating the percentage of inhibition induced by this concentration of GABA revealed a significant decrease in response of APP-PSEN1 neurons (P = 0.0201, unpaired Student's t test) (Fig. 2 F3). This impaired GABAergic receptor response could be due to changes in either $GABA_A$ or $GABA_B$ receptor ($GABA_{A\text{-}B}R$) subtypes. However, a previous electrophysiological report demonstrated that the predominant effect of GABA on LC neurons was mediated *via* $GABA_ARs$, with only significantly higher concentrations (> 600 μM) activating $GABA_BRs$ [63]. We verified this predominant association of GABA with $GABA_ARs$ at the molecular level with immunoreactive clusters for the vesicular GABA transporter (VGAT), a marker of GABA and glycine release sites, being immediately adjacent to cluster immunoreactive for gephyrin, a protein that anchors $GABA_AR$ and GlyRs in postsynaptic junctions (Fig. 2 G1). In contrast, sparse immunoreactivity for $GABA_BR$ was detectable in the LC, which was infrequently

associated with VGAT immunoreactivity (Fig. 2 G2). We therefore focussed further on $GABA_A$Rs and GlyRs.

Impaired α3-$GABA_A$Rs in LC neurons of Alzheimer's patients and APP-PSEN1 mice

Complex changes in the native expression patterns of various $GABA_A$R subunits have been reported in a range of cortical brain regions of Alzheimer's patients [64]. While the complement of $GABA_A$R subunits expressed within the mouse and human LC nucleus has been demonstrated [65], confirmation of the neurochemical identity of the LC cell types expressing specific subunits, at high resolution, remains to be reported. In agreement with a previous report in rat [44], the $GABA_A$R α1 subunit was exclusively expressed in TH immunonegative cells of mouse (Fig. 3 A1-3) and human (Fig. 3 A4). In contrast, immunoreactivity for the α3 subunit in this region of the brainstem strictly overlapped with that of TH, both within the LC nuclear core and the pericoeruleur dendritic regions of the mouse LC (Fig. 3 B1-2), suggesting a significant contribution of this subunit to GABA-mediated regulation of the LC-NA system. The specificity of this labelling pattern was confirmed using tissue from α3 subunit gene deleted mice ($\alpha3^{-/-}$) in which no specific signal was detectable (Fig. 3 B3-4).

High resolution inspection revealed that the majority of α3 subunit immunoreactive clusters were located on plasma membrane surfaces of TH immunopositive neurons immediately adjacent to GABA release sites, identified by immunoreactivity for VGAT in mouse (Fig. 3 C1-3). This pattern of α3 subunit immunoreactivity being concentrated on somatodendritic surfaces of LC NA neurons was replicated in control human samples (Fig. 3 C4). We were unable to detect any specific signal for the α2 subunit (or any other α subunit) in LC neurons, even though we were able to reproduce the quintessential immunoreactivity pattern for this subunit which others have demonstrated in other brain regions such as the hippocampus (SI Fig. 4). TH immunopositive neurons also displayed immunoreactivity for the γ2 (Fig. 3 D1) and β3 (Fig. 3 D2) subunits, with these subunits being closely associated with one another (Fig. 3 D3), Furthermore, the α3 (Fig. 3 E1) and β3 (Fig. 3 E2) subunits were also closely associated with one another (Fig. 3 E3), suggesting that α3-β3-γ2 are the subunit combinations forming the major $GABA_A$R subtype on LC NA neurons.

The importance of α3-$GABA_A$Rs in setting the spontaneous LC FR was confirmed in cells from $\alpha3^{-/-}$ mice, which displayed a significantly higher basal FR compared to WT littermates (P = 0.0048, two-tailed unpaired Student's t test; n = 21 WT cells and 16 $\alpha3^{-/-}$ cells) (Fig. 3 E1). Additionally, the α1/2/3/5-$GABA_A$Rs positive allosteric modulator TP003 [66], which is likely to induce its effects on LC-NA neurons predominantly via α3-β/γ-$GABA_A$Rs due to the absence of other α subunits in this cell type, significantly inhibited the FR of neurons from WT mice (P = 0.0099, two-tailed paired Student's t test; n = 5 cells) (Fig. 3 E2). Presumably this effect of TP003 reflects an action of the drug to enhance the effects of ambient GABA on α3-$GABA_A$Rs. Nevertheless, we cannot exclude an indirect action on adjacent α1 immunopositive, TH-immunonegative LC cells. Collectively, these data suggest that α3-$GABA_A$Rs are integral in setting the basal level of LC neuronal activity, and therefore LC-mediated brain functions and behaviours.

Given the above-mentioned importance of α3-$GABA_A$Rs to LC activity, we next explored their expression and function in APP-PSEN1 mice. Clusters immunoreactive for the α3 subunit were noticeably fewer and smaller in APP-PSEN1 samples, with the majority of the signal located within the cytoplasm of TH immunopositive neurons, rather than the characteristic clustering on plasma membrane surfaces (Fig. 4 A, B). We detected significant decreases in α3 cluster density (P < 0.0001, two-tailed unpaired Student's t test; n = 40 cells from 4 WT animals and n = 50 cells from 5 APP-PSEN1 animals), size (P < 0.0001; two-tailed unpaired Student's t test), fluorescence intensity (P < 0.0001; two-tailed unpaired Student's t test) and percentage of the cell area they covered (P < 0.0001; two-tailed unpaired Student's t test) (Fig. 4 C). In APP-PSEN1 mice, there was a noticeable overlap between pools of α3 and AβO-NU2 immunopositive clusters, both within the cytoplasm of somata and dendrites (Fig. 4D). The functional consequences of this Aβ-altered α3 profile was confirmed by TP003 which significantly decreased the FR of WT cells (P = 0.04, 2-RMA, Sidak's; n = 5 cells), yet had a negligible and non-significant effect in APP-PSEN1 cells (P = 0.9894, 2-RMA, Sidak's; n = 6 cells) (Fig. 4 E).

We sought to confirm these potentially AβO-mediated changes in LC α3 subunit expression using post-mortem LC samples from Alzheimer's patients with demonstrated

Aβ expression in this brain region. The α3 subunit immunoreactivity pattern in such samples was indistinguishable to that obtained in APP-PSEN1 mice, being preferentially located in cytoplasmic compartments occupied by TH immunoreactivity (Fig. 4 F1-6). This preponderance of α3 expression in cytoplasmic rather than membrane domains in Alzheimer's tissue was confirmed by quantifying the degree of colocalization between immunoreactivity for α3 and TH, since TH is expressed exclusively in cytoplasmic compartments. There was a significant difference in the distributions for the α3-TH Manders' colocalization coefficients between control and Alzheimer's samples (*P* <0.0001, Kolmogorov-Smirnov, n = 110 cells from 5 patients in each category) (Fig. 4 F7). In such patients' samples, there was no discernible interaction between immunoreactivity for α3 and Aβ immunopositive plaques (Fig. 4 G). In stark contrast, a significant association between α3 and AβO expression was evident with the considerable overlap between these signals throughout neuronal compartments (Fig. 4 H).

GlyRs and transporters are resistant to AβO pathology in APP-PSEN1 mice and their modulation reverses LC hyperexcitability

We next explored whether the inhibitory drive arising from the LC GlyR-GlyT systems is also influenced by the elevated levels of AβO in APP-PSEN1 mice, firstly by characterising these systems in the WT mouse. Immunoreactivity for GlyR subunits was located throughout somatodendritic surfaces of TH immunopositive neurons, in close proximity to VGAT immunopositive clusters (Fig. 5 A), and their pharmacological activation decreased LC FR (Fig. 5 B). Immunoreactivity for the glycine transporters one and two (GlyT1-2) [67] was concentrated on astrocytic and axonal profiles respectively (Fig. 5 C1-3, D1-3). In addition, inhibition of GlyT1, using ASP2535 [68] (1 μM) (*P* = 0.0015, two-tailed paired Student's t test; n = 8 cells) and GlyT2, using ALX1393 [69](1 μM), (*P* = 0.0006; two-tailed paired Student's t test; n = 11 cells) both significantly decreased LC FR (Fig. 5 C4, D4). Thus, the activity of both GlyRs and GlyT subtypes contributes to setting the basal LC FR.

In light of the above potential to pharmacologically exploit this coexisting inhibitory system as a means to regulating LC excitability, we next characterised the GlyR-GlyT

systems in the APP-PSEN1 model. There were no differences between WT and APP-PSEN1 mice in terms of the pattern (Fig. 6 A1-4), density (P = 0.5299, two-tailed unpaired Student's t test; n = 8 animals) (Fig. 6 A5) and cluster size (P = 0.9250, two-tailed unpaired Student's t test; n = 8 animals) (Fig. 6 A6) of GlyR immunoreactive clusters. Importantly, glycine (30 nM) significantly reduced APP-PSEN1 LC neurons FRs [$F_{(1, 17)}$ = 24.05, P = 0.0001; 2-RMA] in LC FR for both WT (p = 0.0140, Sidak's; n = 10) and APP-PSEN1 (P = 0.0026, Sidak's; n = 9) cells (Fig. 6 A7). Although there was a decrease in GlyT2 immunoreactive cluster density (P = 0.0341, two-tailed unpaired Student's t test; n = 7 animals) (Fig. 6 B1-5) and cluster size (P = 0.0244, two-tailed unpaired Student's t test; n = 7 animals) (Fig. 6 B6), no such changes were detected for GlyT1 (data not shown). This was further confirmed, using the GlyT1 inhibitory ASP2535, which also reversed LC hyperexcitability in LC neurons [F (1, 14) = 54.77, P < 0.0001, 2-RMA) of WT (P = 0.0006, Sidak's; n = 10 cells) and APP-PSEN1 (P = 0.0001, Sidak's; n = 10 cells) mice (Fig. 6 B7). This therefore identifies this pathway as a potential strategy for reversing aberrant levels of LC excitability due to Alzheimer's pathology.

Discussion

The study reveals for the first time, the expression profile of AβO in the LC in Alzheimer's patients, one which is replicated in the APP-PSEN1 mouse model of increased Aβ production. Consequences of this elevated production of Aβ included an array of molecular changes involving immune, neurochemical and metabolic pathways, accompanied by neuronal hyperexcitability and altered NA brain levels. The data provide unique insights into the impact of AβO pathology in a brain region first to exhibit quintessential Alzheimer's pathology.

Importance of AβO in the LC in Alzheimer's

The LC features prominently in assessments of the earliest pathological stages of Alzheimer's, with the predominant characteristic being the presentation of tau tangles in this locus, prior to other brain regions [20]. In stark contrast, the other post mortem pathological hallmark of Alzheimer's, Aβ plaques, is largely overlooked as a contributor to the LC disease spectrum due to the relatively belated presentation of such pathology in this brain region, in most cases only at Braak stages V-VI [21]. However, the importance of the Aβ system in contributing to the initial stages of Alzheimer's could be a significant oversight due to recent evidence indicating that intraneuronal AβO accumulation precedes tau pathology in the entorhinal cortex, which alongside the LC, presents earliest with Alzheimer's pathology [70]. Furthermore, compelling data indicate that AβO, rather than Aβ plaques impart the predominant toxic burden for this pathway [33]. More importantly, especially in terms of the disease phenotype in the LC, converging evidence points to a synergistic role between tau and AβO in mediating Alzheimer's pathology [3, 71, 72]. Indeed, AβO have been shown to enhance, whereas Aβ fibrils reduce, the aggregation of tau [35]. Furthermore, AβO promote the uptake of tau fibril seeds potentiating intracellular aggregation [73] and mediate neurite degeneration [74]. Mechanistic insights into this AβO-tau interaction arise from intriguing new data that demonstrate the involvement of NA, and $\alpha 2_A$ adrenergic receptors ($\alpha 2_A$ARs) in mediating tau hyperphosphorylation and Alzheimer's-related pathology in human and animal samples [75]. Given the significant degree of LC axonal collaterals that provide negative

feedback modulation of LC neuronal activity via $\alpha 2_A$ARs [76] [77], dysregulation of LC hyperexcitability, in combination with locally produced AβO, could set in motion the early levels of tau tangle formation distinctive in this brain region. Therefore, a systematic analysis of the relative temporal expression profiles for the presentation of tau tangle and AβO, rather than Aβ plaques on their own, could provide a more insightful view into the early stages of Alzheimer' disease.

Despite the recognised importance of the LC in Alzheimer's, relatively little is known about the functional changes which occur in the constituent neurons of this nucleus. Whilst various brain imaging techniques have been used to examine the LC in patients at various stages of Alzheimer's, most of these data relate to structural rather than functional changes [78, 79]. The current study provides, to the best of our knowledge, the first analysis of the effects of Aβ-related pathology on the key functional determinant of LC-NA activity, namely spontaneous FR, demonstrating increased activity at the single cell level. This increased FR is likely to negatively impact on a range of behaviours, including cognitive performance [26], a heightened stress response [80] an increase in anxiety-like behaviour [27] and increased wakefulness [23]. This in turn could help to elucidate the neurobiological basis for some of the key behavioural disturbances presented by early-stage Alzheimer's patients, such as enhanced irritability, aggression and disturbances in sleep-wake cycles. Furthermore, if the increased LC FR evident in APP-PSEN1 mice proves to be a consistent feature in the early, pre-cognitive impairment stages of humans with the condition, this could inform recent priorities [29] to develop non-invasive early diagnostic strategies [81, 82].

AβO and the LC inhibitory neurotransmitter systems

A striking finding was the significant impairment in the inhibitory effect of GABA on the tonic FR and the altered expression and function of α3-$GABA_A$Rs of LC neurons in APP-PSEN1 mice. In light of the association of AβO-NU2 immunoreactivity with VGLUT2 signal, we assessed whether there were any changes in glutamatergic synaptic markers in APP-PSEN1 mice. In both APP-PSEN1 mice and Alzheimer's patients, there was a strong overlap between α3-$GABA_A$Rs and AβOs but no association with extracellular insoluble Aβ. Additionally, there were no detectable changes in the levels of expression

of presynaptic (VGLUT2) or postsynaptic (PSD-95) glutamatergic synaptic markers in APP-PSEN1 compared to WT mice (data not shown), suggesting a predominant impact of AβO on inhibitory synapse. Given this increased cytoplasmic and decreased membrane quotient for α3-$GABA_A$Rs, the question therefore arises whether the increased interaction between α3-$GABA_A$Rs and AβOs impairs its trafficking to the membrane or enhances its internalisation from such domains. There is evidence for both mechanisms. The APP-PSEN1 model results in increased expression of amyloid precursor protein (APP) and production of Aβ [83], both of which could impact on the cytoplasmic trafficking and internalisation processes. Firstly, there is a strong interaction between AβO and GABA or $GABA_A$Rs. The application of GABA down-regulates the endocytosis of AβO, thereby decreasing intracellular levels and AβO-induced cytotoxicity in WT mice [84]. Furthermore, there is a bi-directional interaction between AβO and $GABA_A$Rs. AβO impair $GABA_A$R-mediated inhibition [85] by internalising $GABA_A$Rs [16]. In contrast, chronic activation of $GABA_A$Rs decreases $Aβ_{25-35}$-mediated cytotoxicity [86].

An alternative explanation for the decreased α3 membrane expression could be an impairment in the trafficking of newly synthesised subunits to the membrane. $GABA_A$Rs are assembled within the endoplasmic reticulum and transported to the Golgi apparatus for packaging onto vesicles [87]. Subsequently, they are transported to the plasma membrane, from where they diffuse laterally into synapses [88-90]. Several proteins are involved in transporting the $GABA_A$Rs from the Golgi, within transport vesicles, to the plasma membrane and their subsequent phosphorylation. One of these proteins, PLIC-1, facilitates the entry of $GABA_A$R into the secretory pathway [91]. Importantly, PLIC-1 genetically associates with AD [92] and regulates APP, as well as Aβ trafficking and processing [93]. Furthermore, the amount of PLIC-1 directly determines its influence on $GABA_A$R trafficking since its overexpression promotes $GABA_A$R membrane insertion [91]. Since the APP-PSEN1 mouse model is based on increased expression of APP, most probably beyond physiological levels, the expected increased demand for APP and Aβ handling by PLIC-1 in such mice could result in APP processing pathways predominating to the detriment of other systems, including $GABA_A$Rs, resulting in a compromised delivery to plasma membranes. A robust counter-argument to this is that post-mortem samples from Alzheimer's patients exhibited an almost indistinguishable LC α3-$GABA_A$Rs

expression profile to that observed in APP-PSEN1 samples. Indeed, in both mouse and human samples, a significant component of α3 immunoreactivity was located within cytoplasmic compartments, rather than the conventional enrichment on plasma membranes, suggesting that such altered trafficking of these receptors are a phenomenon of the disease itself, rather than the animal model; Finally, a more straightforward explanation could be AβO-mediated damage to the plasma membrane [94], which simply imposes space constraints for receptor insertion.

This strong association between Alzheimer's-related pathology and α3-$GABA_A$Rs is unsurprising. The α3 subunit links a number of brain regions which are known to be adversely affected especially in the early stages of the condition. These include monoaminergic brainstem centres [44, 95, 96] which degenerate with loss of their cortical modulatory presence, fear or stress circuitry such as the amygdala [97] and bed nucleus of the stria terminalis [98], which most likely contribute to the neuropsychiatric symptoms, the olfactory system [98] and the established impairment of olfaction [99], and the entorhinal cortex [100] and its role during the stage of mild cognitive impairment. A likely reason for the vulnerability of these α3-$GABA_A$R centres could be the limited repertoire of $GABA_A$R subtypes expressed by their constituent neurons. For example, compared to cortical pyramidal neurons, which express multiple α subunits and are able to compensate for the loss of individual subunits with limited consequences on neuronal excitability [101], any impairment in α3-$GABA_A$R function is likely to have a tangible effect on the inhibitory modulation of these brain regions. Since many of these neurons already expend a heavy metabolic load in terms of their spontaneous activity and brain wide projections using unmyelinated axons, any impairment in their inhibitory regulation and consequent hyperexcitability is likely to hasten their demise, thereby accounting for their involvement in the AD processes at the earliest stages.

Acknowledgements

We gratefully acknowledge the contribution of the Alzheimer's Society research monitors Chris Penrose, Jane Ward and Julie West for their very constructive discussions throughout the duration of this project.

We would also like to thank the South West Dementia Brain Bank (SWDBB) for providing brain tissue for this study. The SWDBB is part of the Brains for Dementia Research programme, jointly funded by Alzheimer's Research UK and Alzheimer's Society (Brains for Dementia Research) and is supported by BRACE (Bristol Research into Alzheimer's and Care of the Elderly) and the Medical Research Council.

The expert technical assistance of Stewart Gallacher, Daniel Arthur, Scott Rodaway, Angela Scutt, and Andrew Milner is gratefully acknowledged.

We are extremely grateful to Professor Arthur Butt (University of Portsmouth) for providing tissue from GFAP-GFP mice.

Funding

We gratefully acknowledge the support of the Alzheimer's Society (Great Britain), for funding this study with an award to JDS (grant reference 172).

Conflict of interests

The authors declare that the research was conducted in the absence of any commercial or financial relationships that could be construed as a potential conflict of interest.

Ethical Approval

All experiments involving human tissue were in accordance with ethical approval provided by Brains for Dementia Research: REC reference: 08/H0704/128+5; IRAS project ID: 120436; TRID_152.

All procedures involving animal experiments were approved by the Animal Welfare and Ethical Review Body of the University of Portsmouth and were performed by a personal license holder, under a Home Office-issued project license, in accordance with the Animals (Scientific Procedures) Act, 1986 (UK) and associated procedures.

References

1. de Wilde, M.C., et al., *Meta-analysis of synaptic pathology in Alzheimer's disease reveals selective molecular vesicular machinery vulnerability.* Alzheimers Dement, 2016. **12**(6): p. 633-44.
2. DeKosky, S.T. and S.W. Scheff, *Synapse loss in frontal cortex biopsies in Alzheimer's disease: correlation with cognitive severity.* Ann Neurol, 1990. **27**(5): p. 457-64.
3. Spires-Jones, T.L. and B.T. Hyman, *The intersection of amyloid beta and tau at synapses in Alzheimer's disease.* Neuron, 2014. **82**(4): p. 756-71.
4. Jackson, J., et al., *Targeting the Synapse in Alzheimer's Disease.* Front Neurosci, 2019. **13**: p. 735.
5. Colom-Cadena, M., et al., *The clinical promise of biomarkers of synapse damage or loss in Alzheimer's disease.* Alzheimers Res Ther, 2020. **12**(1): p. 21.
6. Viola, K.L. and W.L. Klein, *Amyloid beta oligomers in Alzheimer's disease pathogenesis, treatment, and diagnosis.* Acta Neuropathol, 2015. **129**(2): p. 183-206.
7. Lambert, M.P., et al., *Diffusible, nonfibrillar ligands derived from Abeta1-42 are potent central nervous system neurotoxins.* Proc Natl Acad Sci U S A, 1998. **95**(11): p. 6448-53.
8. Ding, Y., et al., *Amyloid Beta Oligomers Target to Extracellular and Intracellular Neuronal Synaptic Proteins in Alzheimer's Disease.* Front Neurol, 2019. **10**: p. 1140.
9. Koffie, R.M., et al., *Oligomeric amyloid beta associates with postsynaptic densities and correlates with excitatory synapse loss near senile plaques.* Proc Natl Acad Sci U S A, 2009. **106**(10): p. 4012-7.
10. Koffie, R.M., et al., *Apolipoprotein E4 effects in Alzheimer's disease are mediated by synaptotoxic oligomeric amyloid-beta.* Brain, 2012. **135**(Pt 7): p. 2155-68.
11. Lacor, P.N., et al., *Synaptic targeting by Alzheimer's-related amyloid beta oligomers.* J Neurosci, 2004. **24**(45): p. 10191-200.
12. Marcantoni, A., et al., *Abeta42 oligomers up-regulate the excitatory synapses by potentiating presynaptic release while impairing postsynaptic NMDA receptors.* J Physiol, 2020.
13. He, Y., et al., *Amyloid beta oligomers suppress excitatory transmitter release via presynaptic depletion of phosphatidylinositol-4,5-bisphosphate.* Nat Commun, 2019. **10**(1): p. 1193.
14. Calvo-Flores Guzman, B., et al., *Amyloid-Beta1-42 -Induced Increase in GABAergic Tonic Conductance in Mouse Hippocampal CA1 Pyramidal Cells.* Molecules, 2020. **25**(3).
15. Gu, Z., W. Liu, and Z. Yan, *{beta}-Amyloid impairs AMPA receptor trafficking and function by reducing Ca2+/calmodulin-dependent protein kinase II synaptic distribution.* J Biol Chem, 2009. **284**(16): p. 10639-49.

16. Ulrich, D., *Amyloid-beta Impairs Synaptic Inhibition via GABA(A) Receptor Endocytosis.* J Neurosci, 2015. **35**(24): p. 9205-10.
17. Lee, E.B., et al., *Targeting amyloid-beta peptide (Abeta) oligomers by passive immunization with a conformation-selective monoclonal antibody improves learning and memory in Abeta precursor protein (APP) transgenic mice.* J Biol Chem, 2006. **281**(7): p. 4292-9.
18. Mc Donald, J.M., et al., *The presence of sodium dodecyl sulphate-stable Abeta dimers is strongly associated with Alzheimer-type dementia.* Brain, 2010. **133**(Pt 5): p. 1328-41.
19. Bao, F., et al., *Different beta-amyloid oligomer assemblies in Alzheimer brains correlate with age of disease onset and impaired cholinergic activity.* Neurobiol Aging, 2012. **33**(4): p. 825 e1-13.
20. Weinshenker, D., *Long Road to Ruin: Noradrenergic Dysfunction in Neurodegenerative Disease.* Trends Neurosci, 2018. **41**(4): p. 211-223.
21. Braak, H., et al., *Stages of the pathologic process in Alzheimer disease: age categories from 1 to 100 years.* J Neuropathol Exp Neurol, 2011. **70**(11): p. 960-9.
22. Sara, S.J., *Locus Coeruleus in time with the making of memories.* Curr Opin Neurobiol, 2015. **35**: p. 87-94.
23. Carter, M.E., et al., *Tuning arousal with optogenetic modulation of locus coeruleus neurons.* Nat Neurosci, 2010. **13**(12): p. 1526-33.
24. Itoi, K. and N. Sugimoto, *The brainstem noradrenergic systems in stress, anxiety and depression.* J Neuroendocrinol, 2010. **22**(5): p. 355-61.
25. Valentino, R.J. and E. Van Bockstaele, *Convergent regulation of locus coeruleus activity as an adaptive response to stress.* Eur J Pharmacol, 2008. **583**(2-3): p. 194-203.
26. Usher, M., et al., *The role of locus coeruleus in the regulation of cognitive performance.* Science, 1999. **283**(5401): p. 549-54.
27. McCall, J.G., et al., *CRH Engagement of the Locus Coeruleus Noradrenergic System Mediates Stress-Induced Anxiety.* Neuron, 2015. **87**(3): p. 605-20.
28. Sanchez-Padilla, J., et al., *Mitochondrial oxidant stress in locus coeruleus is regulated by activity and nitric oxide synthase.* Nat Neurosci, 2014. **17**(6): p. 832-40.
29. Betts, M.J., et al., *Locus coeruleus imaging as a biomarker for noradrenergic dysfunction in neurodegenerative diseases.* Brain, 2019. **142**: p. 2558-2571.
30. Ross, J.A., et al., *Localization of amyloid beta peptides to locus coeruleus and medial prefrontal cortex in corticotropin releasing factor overexpressing male and female mice.* Brain Struct Funct, 2019. **224**(7): p. 2385-2405.

31. Ross, J.A., et al., *Localization of endogenous amyloid-beta to the coeruleo-cortical pathway: consequences of noradrenergic depletion.* Brain Struct Funct, 2018. **223**(1): p. 267-284.
32. Thal, D.R., et al., *Phases of A beta-deposition in the human brain and its relevance for the development of AD.* Neurology, 2002. **58**(12): p. 1791-800.
33. Ghag, G., et al., *Soluble tau aggregates, not large fibrils, are the toxic species that display seeding and cross-seeding behavior.* Protein Science, 2018. **27**(11): p. 1901-1909.
34. Cline, E.N., et al., *The Amyloid-beta Oligomer Hypothesis: Beginning of the Third Decade.* J Alzheimers Dis, 2018. **64**(s1): p. S567-S610.
35. Shin, W.S., et al., *Different Amyloid-beta Self-Assemblies Have Distinct Effects on Intracellular Tau Aggregation.* Front Mol Neurosci, 2019. **12**: p. 268.
36. Pickett, E.K., et al., *Amyloid Beta and Tau Cooperate to Cause Reversible Behavioral and Transcriptional Deficits in a Model of Alzheimer's Disease.* Cell Rep, 2019. **29**(11): p. 3592-3604 e5.
37. Chan-Palay, V. and E. Asan, *Alterations in catecholamine neurons of the locus coeruleus in senile dementia of the Alzheimer type and in Parkinson's disease with and without dementia and depression.* J Comp Neurol, 1989. **287**(3): p. 373-92.
38. De Felice, F.G., et al., *Abeta oligomers induce neuronal oxidative stress through an N-methyl-D-aspartate receptor-dependent mechanism that is blocked by the Alzheimer drug memantine.* J Biol Chem, 2007. **282**(15): p. 11590-601.
39. Heneka, M.T., et al., *Locus ceruleus controls Alzheimer's disease pathology by modulating microglial functions through norepinephrine.* Proc Natl Acad Sci U S A, 2010. **107**(13): p. 6058-63.
40. Heneka, M.T., et al., *Locus ceruleus degeneration promotes Alzheimer pathogenesis in amyloid precursor protein 23 transgenic mice.* J Neurosci, 2006. **26**(5): p. 1343-54.
41. Jankowsky, J.L., et al., *Mutant presenilins specifically elevate the levels of the 42 residue beta-amyloid peptide in vivo: evidence for augmentation of a 42-specific gamma secretase.* Hum Mol Genet, 2004. **13**(2): p. 159-70.
42. Yee, B.K., et al., *A schizophrenia-related sensorimotor deficit links alpha 3-containing GABAA receptors to a dopamine hyperfunction.* Proc Natl Acad Sci U S A, 2005. **102**(47): p. 17154-9.
43. Lalo, U., et al., *NMDA receptors mediate neuron-to-glia signaling in mouse cortical astrocytes.* J Neurosci, 2006. **26**(10): p. 2673-83.
44. Corteen, N.L., et al., *Localization of GABA-A receptor alpha subunits on neurochemically distinct cell types in the rat locus coeruleus.* Eur J Neurosci, 2011. **34**(2): p. 250-62.
45. Campos-Lira, E., et al., *Dynamic Modulation of Mouse Locus Coeruleus Neurons by Vasopressin 1a and 1b Receptors.* Front Neurosci, 2018. **12**: p. 919.

46. Swinny, J.D., et al., *Neonatal rearing conditions distinctly shape locus coeruleus neuronal activity, dendritic arborization, and sensitivity to corticotrophin-releasing factor.* Int J Neuropsychopharmacol, 2010. **13**(4): p. 515-25.
47. Seifi, M., et al., *GABAA Receptor Subtypes Regulate Stress-Induced Colon Inflammation in Mice.* Gastroenterology, 2018. **155**(3): p. 852-864 e3.
48. Okano, H.J. and R.B. Darnell, *A hierarchy of Hu RNA binding proteins in developing and adult neurons.* J Neurosci, 1997. **17**(9): p. 3024-37.
49. Lambert, M.P., et al., *Monoclonal antibodies that target pathological assemblies of Abeta.* J Neurochem, 2007. **100**(1): p. 23-35.
50. Hansson Petersen, C.A., et al., *The amyloid beta-peptide is imported into mitochondria via the TOM import machinery and localized to mitochondrial cristae.* Proc Natl Acad Sci U S A, 2008. **105**(35): p. 13145-50.
51. Wiegand, G. and S.J. Remington, *Citrate synthase: structure, control, and mechanism.* Annu Rev Biophys Biophys Chem, 1986. **15**: p. 97-117.
52. Manders, E.M.M., F.J. Verbeek, and J.A. Aten, *Measurement of Colocalization of Objects in Dual-Color Confocal Images.* Journal of Microscopy-Oxford, 1993. **169**: p. 375-382.
53. Aaron, J.S., A.B. Taylor, and T.L. Chew, *Image co-localization - co-occurrence versus correlation.* J Cell Sci, 2018. **131**(3).
54. Picone, P., et al., *Mitochondrial dysfunction: different routes to Alzheimer's disease therapy.* Oxid Med Cell Longev, 2014. **2014**: p. 780179.
55. Du, S., et al., *Curcumin Alleviates beta Amyloid-Induced Neurotoxicity in HT22 Cells via Upregulating SOD2.* J Mol Neurosci, 2019. **67**(4): p. 540-549.
56. Majd, S. and J.H.T. Power, *Oxidative Stress and Decreased Mitochondrial Superoxide Dismutase 2 and Peroxiredoxins 1 and 4 Based Mechanism of Concurrent Activation of AMPK and mTOR in Alzheimer's Disease.* Curr Alzheimer Res, 2018. **15**(8): p. 764-776.
57. Heneka, M.T., et al., *Neuroinflammation in Alzheimer's disease.* Lancet Neurol, 2015. **14**(4): p. 388-405.
58. Welikovitch, L.A., et al., *Early intraneuronal amyloid triggers neuron-derived inflammatory signaling in APP transgenic rats and human brain.* Proc Natl Acad Sci U S A, 2020. **117**(12): p. 6844-6854.
59. Olmos-Alonso, A., et al., *Pharmacological targeting of CSF1R inhibits microglial proliferation and prevents the progression of Alzheimer's-like pathology.* Brain, 2016. **139**(Pt 3): p. 891-907.

60. Luo, J., et al., *Colony-stimulating factor 1 receptor (CSF1R) signaling in injured neurons facilitates protection and survival.* J Exp Med, 2013. **210**(1): p. 157-72.
61. Bajjalieh, S.M., et al., *Differential expression of synaptic vesicle protein 2 (SV2) isoforms.* J Neurosci, 1994. **14**(9): p. 5223-35.
62. Somogyi, J. and I.J. Llewellyn-Smith, *Patterns of colocalization of GABA, glutamate and glycine immunoreactivities in terminals that synapse on dendrites of noradrenergic neurons in rat locus coeruleus.* Eur J Neurosci, 2001. **14**(2): p. 219-28.
63. Osmanovic, S.S. and S.A. Shefner, *gamma-Aminobutyric acid responses in rat locus coeruleus neurones in vitro: a current-clamp and voltage-clamp study.* J Physiol, 1990. **421**: p. 151-70.
64. Kwakowsky, A., et al., *GABAA receptor subunit expression changes in the human Alzheimer's disease hippocampus, subiculum, entorhinal cortex and superior temporal gyrus.* J Neurochem, 2018. **145**(5): p. 374-392.
65. Waldvogel, H.J., et al., *Differential localization of gamma-aminobutyric acid type A and glycine receptor subunits and gephyrin in the human pons, medulla oblongata and uppermost cervical segment of the spinal cord: an immunohistochemical study.* J Comp Neurol, 2010. **518**(3): p. 305-28.
66. Neumann, E., et al., *TP003 is a non-selective benzodiazepine site agonist that induces anxiolysis via alpha2GABAA receptors.* Neuropharmacology, 2018. **143**: p. 71-78.
67. Eulenburg, V., et al., *Glycine transporters: essential regulators of neurotransmission.* Trends Biochem Sci, 2005. **30**(6): p. 325-33.
68. Harada, K., et al., *A novel glycine transporter-1 (GlyT1) inhibitor, ASP2535 (4-[3-isopropyl-5-(6-phenyl-3-pyridyl)-4H-1,2,4-triazol-4-yl]-2,1,3-benzoxadiazol e), improves cognition in animal models of cognitive impairment in schizophrenia and Alzheimer's disease.* Eur J Pharmacol, 2012. **685**(1-3): p. 59-69.
69. Eckle, V.S. and B. Antkowiak, *ALX 1393 inhibits spontaneous network activity by inducing glycinergic tonic currents in the spinal ventral horn.* Neuroscience, 2013. **253**: p. 165-71.
70. Welikovitch, L.A., et al., *Evidence of intraneuronal Abeta accumulation preceding tau pathology in the entorhinal cortex.* Acta Neuropathol, 2018. **136**(6): p. 901-917.
71. Crimins, J.L., et al., *The intersection of amyloid beta and tau in glutamatergic synaptic dysfunction and collapse in Alzheimer's disease.* Ageing Res Rev, 2013. **12**(3): p. 757-63.
72. Ittner, L.M. and J. Gotz, *Amyloid-beta and tau--a toxic pas de deux in Alzheimer's disease.* Nat Rev Neurosci, 2011. **12**(2): p. 65-72.

73. Shin, W.S., et al., *Amyloid beta-protein oligomers promote the uptake of tau fibril seeds potentiating intracellular tau aggregation.* Alzheimers Res Ther, 2019. **11**(1): p. 86.
74. Jin, M., et al., *Soluble amyloid beta-protein dimers isolated from Alzheimer cortex directly induce Tau hyperphosphorylation and neuritic degeneration.* Proc Natl Acad Sci U S A, 2011. **108**(14): p. 5819-24.
75. Zhang, F., et al., *beta-amyloid redirects norepinephrine signaling to activate the pathogenic GSK3beta/tau cascade.* Sci Transl Med, 2020. **12**(526).
76. Aghajanian, G.K., J.M. Cedarbaum, and R.Y. Wang, *Evidence for norepinephrine-mediated collateral inhibition of locus coeruleus neurons.* Brain Res, 1977. **136**(3): p. 570-7.
77. Cedarbaum, J.M. and G.K. Aghajanian, *Noradrenergic neurons of the locus coeruleus: inhibition by epinephrine and activation by the alpha-antagonist piperoxane.* Brain Res, 1976. **112**(2): p. 413-9.
78. Peterson, A.C. and C.R. Li, *Noradrenergic Dysfunction in Alzheimer's and Parkinson's Diseases-An Overview of Imaging Studies.* Front Aging Neurosci, 2018. **10**: p. 127.
79. Betts, M.J., et al., *Locus coeruleus imaging as a biomarker for noradrenergic dysfunction in neurodegenerative diseases.* Brain, 2019.
80. Abercrombie, E.D. and B.L. Jacobs, *Single-unit response of noradrenergic neurons in the locus coeruleus of freely moving cats. I. Acutely presented stressful and nonstressful stimuli.* J Neurosci, 1987. **7**(9): p. 2837-43.
81. Elman, J.A., et al., *Task-evoked pupil dilation and BOLD variance as indicators of locus coeruleus dysfunction.* Cortex, 2017. **97**: p. 60-69.
82. Granholm, E.L., et al., *Pupillary Responses as a Biomarker of Early Risk for Alzheimer's Disease.* J Alzheimers Dis, 2017. **56**(4): p. 1419-1428.
83. Borchelt, D.R., et al., *Accelerated amyloid deposition in the brains of transgenic mice coexpressing mutant presenilin 1 and amyloid precursor proteins.* Neuron, 1997. **19**(4): p. 939-45.
84. Sun, X., et al., *GABA attenuates amyloid toxicity by downregulating its endocytosis and improves cognitive impairment.* J Alzheimers Dis, 2012. **31**(3): p. 635-49.
85. Hu, B., C. Geng, and X.Y. Hou, *Oligomeric amyloid-beta peptide disrupts olfactory information output by impairment of local inhibitory circuits in rat olfactory bulb.* Neurobiol Aging, 2017. **51**: p. 113-121.
86. Lee, B.Y., J.Y. Ban, and Y.H. Seong, *Chronic stimulation of GABAA receptor with muscimol reduces amyloid beta protein (25-35)-induced neurotoxicity in cultured rat cortical cells.* Neurosci Res, 2005. **52**(4): p. 347-56.

87. Comenencia-Ortiz, E., S.J. Moss, and P.A. Davies, *Phosphorylation of GABA(A) receptors influences receptor trafficking and neurosteroid actions.* Psychopharmacology, 2014. **231**(17): p. 3453-3465.
88. Thomas, P., et al., *Dynamic mobility of functional GABAA receptors at inhibitory synapses.* Nat Neurosci, 2005. **8**(7): p. 889-897.
89. Jacob, T.C., et al., *Gephyrin Regulates the Cell Surface Dynamics of Synaptic GABAA Receptors.* The Journal of Neuroscience, 2005. **25**(45): p. 10469-10478.
90. Jacob, T.C., S.J. Moss, and R. Jurd, *GABA(A) receptor trafficking and its role in the dynamic modulation of neuronal inhibition.* Nature reviews. Neuroscience, 2008. **9**(5): p. 331-343.
91. Bedford, F.K., et al., *GABA(A) receptor cell surface number and subunit stability are regulated by the ubiquitin-like protein Plic-1.* Nat Neurosci, 2001. **4**(9): p. 908-16.
92. Bertram, L., et al., *Family-based association between Alzheimer's disease and variants in UBQLN1.* N Engl J Med, 2005. **352**(9): p. 884-94.
93. Hiltunen, M., et al., *Ubiquilin 1 modulates amyloid precursor protein trafficking and Abeta secretion.* J Biol Chem, 2006. **281**(43): p. 32240-53.
94. Julien, C., et al., *In vivo induction of membrane damage by beta-amyloid peptide oligomers.* Acta Neuropathol Commun, 2018. **6**(1): p. 131.
95. Gao, B., et al., *Neuron-specific expression of GABAA-receptor subtypes: differential association of the alpha 1- and alpha 3-subunits with serotonergic and GABAergic neurons.* Neuroscience, 1993. **54**(4): p. 881-92.
96. Corteen, N.L., et al., *Localisation and stress-induced plasticity of GABAA receptor subunits within the cellular networks of the mouse dorsal raphe nucleus.* Brain Struct Funct, 2015. **220**(5): p. 2739-63.
97. Marowsky, A., et al., *Tonic inhibition in principal cells of the amygdala: a central role for alpha3 subunit-containing GABAA receptors.* J Neurosci, 2012. **32**(25): p. 8611-9.
98. Hortnagl, H., et al., *Patterns of mRNA and protein expression for 12 GABAA receptor subunits in the mouse brain.* Neuroscience, 2013. **236**: p. 345-72.
99. Daulatzai, M.A., *Olfactory dysfunction: its early temporal relationship and neural correlates in the pathogenesis of Alzheimer's disease.* J Neural Transm (Vienna), 2015. **122**(10): p. 1475-97.
100. Berggaard, N., et al., *Spatiotemporal Distribution of GABAA Receptor Subunits Within Layer II of Mouse Medial Entorhinal Cortex: Implications for Grid Cell Excitability.* Front Neuroanat, 2018. **12**: p. 46.
101. Sur, C., et al., *Loss of the major GABA(A) receptor subtype in the brain is not lethal in mice.* J Neurosci, 2001. **21**(10): p. 3409-18.

Table 1

Summary of basic membrane characteristics of recorded noradrenergic LC neurons in WT and APP-PSEN1 mice. Data are presented as the mean ± SEM, n = number of cells used per parameter.

Parameter (n) = number of cells	**WT**	**APP-PSEN1**	***P* (unpaired Student's *t* test)**
Spontaneous FR, Hz (n)	2.57 ± 0.26 (32)	4.37 ± 0.30 (35)	< 0.0001
Resting membrane potential, mV (n)	-53.20 ± 1.23 (12)	-52.76 ± 1.29 (9)	0.8083
Cell capacitance, pF (n)	30.45 ± 1.25 (12)	30.76 ± 1.86 (11)	0.8884
Threshold for action potential, mV (n)	-43.27 ± 1.71 (11)	-44.33 ± 2.49 (9)	0.7225
Amplitude of action potential, mV (n)	62.82 ± 2.39 (11)	66.11 ± 3.05 (9)	0.3997
Cells spontaneously firing action potentials, % (n)	94.12 (34)	97.22 (36)	NA
Input resistance, MΩ (n)	386.6 ± 0.05 (12)	295.4 ± 0.04 (8)	0.1840
Time constant, ms (n)	66.3 ± 11.45 (12)	35.88 ± 3.48 (9)	0.0380

Figure Legends

Figure 1

Immunolocalization of oligomeric amyloid β (Aβ) within the LC of Alzheimer's patients and APP-PSEN1 mice. (A1) in post-mortem samples from Alzheimer's patients, immunoreactivity for an antibody that recognises both fibrillar and oligomeric forms of Aβ presents exclusively as extracellular plaques (arrowheads) with no intracellular signal evident in LC noradrenergic neurons, identified by immunoreactivity for tyrosine hydroxylase (TH) (asterisk). (A2-3) in APP-PSEN1 mice, immunoreactivity for Aβ is concentrated within LC noradrenergic neurons, with no evidence of extracellular plaques. (A4) is a magnified view of the boxed area in (A 2-3) demonstrating that Aβ is also expressed in non-noradrenergic LC neurons (arrowheads). n = 5 Alzheimer's-control subjects, at least 5 APP-PSEN1-WT mice. (B) in LC samples from Alzheimer's patients, immunoreactivity for an antibody specific for Aβ oligomers (AβO), termed AβO-NU2, shows enrichments within TH-immunopositive somata, together with extracellular clusters. n = 5 Alzheimer's-control subjects. (C1-3) in LC samples from APP-PSEN1 mice, an overview of immunoreactivity for AβO-NU2 reveals its enrichment throughout LC neurons, mirroring the expression pattern in Alzheimer's samples. However, some TH-immunopositive cells do not exhibit immunoreactivity for AβO-NU2 (arrowheads). (C4) is a magnified view demonstrating that AβO-NU2 immunoreactivity is located within somata of LC neurons and profiles resembling axons (arrowheads). Individual extracellular clusters are also evident. n = > 5 APP-PSEN1 mice. (D) immunoreactivity for a different AβO antibody, termed NU1 that recognises oligomers different in size to NU2, in the LC of APP-PSEN1 mice. Note the significant variation in the intensity of the signal across different TH-immunopositive somata, with some cells (arrowheads) apparently devoid of any immunoreactivity. n = > 5 APP-PSEN1 mice. (E1-2) cytoplasmic AβO-NU1 signal is closely associated (arrowheads) with mitochondria, identified by immunoreactivity for the mitochondria matrix marker citrate synthase. A significant degree of overlap is evident in extracellular clusters which could represent axon terminals. n = > 5 APP-PSEN1 mice. (E3) there is a positive association between the location of immunoreactivity for AβO-

NU1 and citrate synthase, with Manders' representing the degree of co-occurrence of overlapping pixels and Pearson's the correlation of the intensity of overlapping pixels, n = 50 cells. (F1-2) in the LC of APP-PSEN1 mice, cytoplasmic AβO-NU2 signal is also located in close proximity to citrate synthase. n = > 5 APP-PSEN1 mice. (F3) there is a positive association between the location of immunoreactivity for AβO-NU2 and citrate synthase, with Manders' representing the degree of co-occurrence of overlapping pixels and Pearson's the correlation of the intensity of overlapping pixels, n = 50 cells. (G) and (H), in the LC of APP-PSEN1 mice, cytoplasmic immunoreactivity for both AβO-NU1 and AβO-NU2 is closely associated with signal for superoxide dismutase 2 (SOD2), a key mitochondrial enzyme in oxidative stress. n = > 5 APP-PSEN1 mice. For both (G3) and (H3), n = 50 cells. (I 1-6) representative images of the relative levels of immunoreactivity for superoxide dismutase 2 (SOD2) in the LC of WT and APP-PSEN1 mice. Note the significant decrease in APP-PSEN1 samples of the intensity of signal for this enzyme which is protective against oxidative stress. (I7) quantification of SOD2 immunofluorescence intensity in WT and APP-PSEN1 samples. Two-tailed unpaired Student's *t* test, n = 5 animals. (J1-2) show immunoreactivity for IBA1, a marker of activated microglia, in the LC of WT and APP-PSEN1 respectively, reacted and imaged under identical conditions. There is an apparent increase in the density of profiles in the APP-PSEN1 image, suggestive of enhanced microglial activation. This increased IBA1 expression in APP-PSEN1 samples was confirmed at the (J3) mRNA level (two-tailed unpaired Student's *t* test, n = 5 animals) and (J4) cellular level (two-tailed unpaired Student's *t* test, n = 10 animals). (J4-7) comparative LC and hippocampal mRNA expression levels of the cytokines colony stimulating factor 1 (CSF1), interleukin 1 β (IL1β) and chemokine (C-C motif) ligand 3 (CCL3) respectively. Two way (genotype and brain region) ANOVA with Sidak's post hoc test, n = 5 animals. All immunohistochemical images presented represent a single optical section. The symbols represent the individual data points, the bars represent the means and the error bars the SEM. * = $P < 0.05$. Scale bars: (A1) 30 μm; (A2-3) 50 μm; (A4) 15 μm; (B1-2) 15 μm; (C1-3) 100 μm; (C4) 15 μm; (D) 60 μm; (E, F, G, H 1-2) 15 μm; (I 1-2, 4-5) 100 μm; (I 3, 6) 15 μm; (J) 15 μm.

Figure 2

Association of AβO with synapses and LC neuronal excitability in APP-PSEN1. (A) extracellular AβO-NU2 immunoreactivity is located in close apposition to clusters immunopositive for the pan-presynaptic marker protein, synaptic vesicle glycoprotein 2A (SV2A) (arrowheads), indicating expression at synaptic junctions. (A4) is a magnified view of the boxed areas in (A1-3). n = > 5 APP-PSEN1 mice. (B) extracellular AβO-NU2 immunoreactive clusters are closely associated with inhibitory axon terminals, identified by immunoreactivity for the vesicular GABA transporter (VGAT) (arrowheads), indicating expression in close proximity to GABAergic synapses. (B4) is a magnified view of the boxed areas in (B1-3). n = > 5 APP-PSEN1 mice. (C) extracellular AβO-NU2 immunoreactive clusters are closely associated excitatory axon terminals, identified by immunoreactivity for the vesicular glutamate transporter 2 (VGLUT2) (arrowheads), indicating expression in close proximity to glutamatergic synapses. (C4) is a magnified view of the boxed areas in (C1-3). n = > 5 APP-PSEN1 mice. (D1) representative image of a recorded neuron, loaded with biocytin during the recording, and processed post-hoc for TH immunohistochemistry, confirming that recorded neurons were located within the LC and were noradrenergic.

(D2) representative traces of the spontaneous firing rates (FRs) of LC noradrenergic neurons in WT and APP-PSEN1 mice. Note the significantly higher FR in the trace for APP-PSEN1. (D3) quantification of the spontaneous FR (Hz) of LC noradrenergic neurons in WT and APP-PSEN1 mice. The data points represent individual cells. Two-tailed unpaired Student's *t* test, n = 32 cells for WT and 35 for APP-PSEN1.

(D4) quantification of the membrane time constant for WT and APP-PSEN1 mice. The data points represent individual cells. Two-tailed unpaired Student's *t* test, n = 12 cells for WT and 9 for APP-PSEN1. (E) quantification of the concentration of noradrenaline in the LC and hippocampus of WT and APP-PSEN1 mice using an ELISA for NA. The data points represent individual mice. Two way (genotype and brain region) ANOVA, with Sidak's post hoc test, n = 5 animals. (F1) concentration-dependent effect of the inhibitory role of GABA on spontaneous LC FR in WT mice, n = 4-7 cells per GABA concentration. (F2) diminished inhibitory effect of GABA in LC neurons form APP-PSEN1 mice. The data points represent individual cells. Two way (genotype and drug) ANOVA, n = 7 cells for WT and 13 for APP-PSEN1. (F3) percentage decrease in spontaneous LC FR following the application of 100 nm GABA in WT and APP-PSEN1 mice. The data points

represent individual mice. Two-tailed unpaired Student's *t* test, n = 7 cells for WT and 13 for APP-PSEN1. (G1) demonstration that the majority of GABA release sites, identified by immunoreactivity for the vesicular GABA transporter (VGAT) are located adjacent to domains containing putative $GABA_A$ and glycine receptors, identified by immunoreactivity for the $GABA_A$ and glycine receptor anchoring protein gephyrin. (G2) in contrast to (G1), sparse clusters immunoreactive for the $GABA_B$ receptor are located on TH-immunopositive profiles which rarely are located adjacent to VGAT-immunoreactive clusters. All immunohistochemical images presented represent a single optical section. The symbols represent the individual data points, the bars represent the means and the error bars the SEM. * = $P < 0.05$.

Scale bars: (A1-3) 5 µm; (A4) 1 µm; (B1-3) 5 µm; (B4) 3 µm; (C) 2 µm; (D1) 10 µm; (D2) horizontal, 500 ms, vertical 20 mV; (G1) 10 µm; (G2) 5 µm.

Figure 3

Demonstration of native $GABA_A$ receptor ($GABA_AR$) subtypes expressed in mouse and human LC neurons. (A1) TH immunoreactivity identifying noradrenergic neurons in the mouse LC. (A2) shows immunoreactivity for the $GABA_AR$ α1 subunit in the corresponding field of view. (A3) is a magnified overlay of the boxed areas in (A1 and A2) showing α1 immunoreactivity is expressed in LC somata (asterisk) and dendrites of profiles which are TH-immunonegative. (A4) in the human LC, α1 immunoreactivity is also expressed exclusively in TH-immunonegative cells (asterisks). n = 5 human control subjects and > 5 WT mice. (B) overview of LC α3 subunit immunoreactivity in WT and α3 gene deleted mice ($\alpha3^{-/-}$), thereby confirming the specificity of the α3 antibody used, n = 4 WT and $\alpha3^{-/-}$animals. (C1-3) high resolution immunolocalization demonstrating that in the mouse LC, α3 immunoreactivity is concentrated on somatic and dendritic surfaces adjacent to GABA release sites (arrowheads), identified by immunoreactivity for VGAT. (C4), in the human LC, α3 immunoreactivity is also enriched on the somatic and dendritic (arrowheads) of noradrenergic neurons. n = 5 human control subjects and > 5 WT mice. Mouse LC noradrenergic neurons also express (D1) the γ2 and (D2) β3 subunits, which (D3) are closely associated with one another (arrowheads). (E1) α3 immunoreactivity is closely associated with immunoreactivity for (E2-3) the β3 subunit (arrowheads). (F) α3-containing $GABA_ARs$ (α3-$GABA_ARs$) contribute to the basal FR of LC neurons, with (E1)

the deletion of this subunit resulting in a significant increase (two-tailed unpaired Student's t test, n = 32 WT cells, 16 $\alpha3^{-/-}$ cells), whilst (E2) its pharmacological activation resulting in a significant decrease (two-tailed paired Student's *t* test, n = 5 cells). All immunohistochemical images presented represent a single optical section. The symbols represent the individual data points, the bars represent the means and the error bars the SEM. * = $P < 0.05$. Scale bars: (A1-2) 30 µm; (A3) 10 µm; (A4) 20 µm; (B) 100 µm; (C) 15 µm; (D) 10 µm; (E) 5 µm.

Figure 4

Interaction of AβO and α3-$GABA_A$Rs in the LC of Alzheimer's patients and APP-PSEN1 mice. (A) representative image of the immunoreactivity pattern of the α3 subunit in the LC of a WT mouse. (B) representative image of the immunoreactivity pattern of the α3 subunit in the LC of an APP-PSEN1 mouse, processed and imaged under conditions identical to WT samples. Note the sparse localisation of signal on somato-dendritic plasma membranes, with the majority of the signal preferentially located in cytoplasmic compartments. n = > 5 APP-PSEN1-WT mice. Quantification of the (C1) density, (C2) size, (C3) mean fluorescence intensity of α3 subunit immunoreactive clusters and (C4) percentage of cell area they occupy, in the LC of WT and APP-PSEN1 mice. Two-tailed unpaired Student's t test, n = 40 cells for WT, and 50 for APP-PSEN1. (D) shows that in LC somata and dendrites of APP-PSEN1 mice, pools of AβO-NU2 immunopositive clusters overlap with clusters immunopositive the α3 subunit (arrowheads). (D4) is a magnified view of the boxed areas in (D1-3). (E) differences in the inhibitory effect of the α1/3/5-$GABA_A$R positive allosteric modulator TP003 in LC neurons from WT and APP-PSEN1 mice. While TP003 robustly inhibits LC FR in WT cells, there is no significant effect in cells from APP-PSEN1 mice. The data points represent individual cells. Two-way (genotype and drug) repeated measures ANOVA, n = 5 cells. (F1-3) representative image of immunoreactivity for the α3 subunit in the LC of control human tissue. (F4-6) representative image of immunoreactivity for the α3 subunit in the LC of an Alzheimer's patient. Note how the α3 signal in patient material mirrors that of the APP-PSEN1 mouse, being predominantly restricted to cytoplasmic compartments, with significantly lower levels evident on plasma membrane compartments. n = 5 Alzheimer's subjects.

(F7) quantification of the association between immunoreactivity for the α3 subunit and TH, as a measure of cytoplasmically located α3 subunit, using the Manders' coefficient of the co-occurrence of overlapping pixels. The data points represent individual cells. $P > 0.05$, Kolmogorov–Smirnov test, n = 110 cells per group. (G) representative image showing the lack of an association between signal for fibrillar Aβ (arrowheads) and the α3 subunit in the LC of Alzheimer's patients. n = 5 Alzheimer's subjects. (H) representative image showing that in the LC of Alzheimer's patients, immunoreactivity for AβO-NU2 and the α3 subunit are located in close proximity to one another, in a pattern that mirrors expression in APP-PSEN1 mice. n = 5 Alzheimer's subjects. All immunohistochemical images presented represent a single optical section. The symbols represent the individual data points, the bars represent the means and the error bars the SEM. * = $P < 0.05$. Scale bars: (A, B, D1-3) 10 μm; (D4) 5 μm; (F1-2; F4-5) 15 μm; (F3, F6) 6 μm; (G) 15 μm; (H) 20 μm.

Figure 5

Demonstration of native glycine receptor and transporter subtypes expressed in mouse LC neurons. (A) immunoreactivity for an antibody that recognises all GlyR α subunits and its close association with immunoreactivity for the vesicular GABA transporter (VGAT). n = > 5 WT mice. (B) concentration-dependent inhibitory effect of applied glycine on spontaneous LC FR. n = 10 cells. (C1-3) immunoreactivity for the glycine transporter 1 (GlyT1) is associated with astrocytic profiles, identified by immunoreactivity for glial fibrillary acid protein (GFAP). n = > 5 WT mice. (C4) quantification of the frequency (Hz) of LC noradrenergic neuronal spontaneous firing before and after the bath application of 1 μM ASP-2535, an inhibitor of GlyT1. Two-tailed paired Student's *t* test, n = 8 cells. (D1-3) immunoreactivity for the glycine transporter 2 (GlyT2) is associated with inhibitory axon terminals, identified by the immunoreactivity for VGAT. n = > 5 WT mice. (D4) quantification of the frequency (Hz) of LC noradrenergic spontaneous firing before and after the bath application of 1 μM ALX-1393, an inhibitor of GlyT2. Two-tailed paired Student's *t* test, n = 8 cells. All immunohistochemical images presented represent a single optical section. The symbols represent the individual data points, the bars

represent the means and the error bars the SEM. * = $P < 0.05$. Scale bars: (A) 10 μm; (C, D) 20 μm.

Figure 6

Quantification of the changes in the expression and function of GlyRs and GlyTs in LC neurons of the APP-PSEN1 mice. (A1) and (A2) show representative images of the pattern and intensity of TH and GlyR immunoreactivity, respectively, in tissue from a WT mouse. (A3) and (A4) show the comparative TH and GlyR immunoreactivity patterns, respectively, in in tissue from an APP-PSEN1 mouse. Note that samples for (A1-2) and (A3-4) were reacted and imaged under identical conditions. Quantification of GlyR immunoreactive cluster (A5) density and (A6) area. (A7) quantification of the comparative inhibitory effects of applied glycine (30 nM) on spontaneous LC FR in WT and APP-PSEN1 cells. (A5, 6) Two-tailed unpaired Student's t test. (A7) Two way (genotype and drug) ANOVA with repeated measures, n = 10 WT cells and 9 APP-PSEN1 cells. (B1) and (B2) show representative images of the pattern and intensity of TH and GlyT2 immunoreactivity, respectively, in tissue from a WT mouse. (B3) and (B4) show the comparative TH and GlyT2 immunoreactivity patterns, respectively, in in tissue from an APP-PSEN1 mouse. Note that samples for (B1-2) and (B3-4) were reacted and imaged under identical conditions. Quantification of GlyT2 immunoreactive cluster (B5) density and (B6) area. (B7) quantification of the comparative inhibitory effects of applied glycine transporter inhibitor ASP 1393 (1 μM) on spontaneous LC FR in WT and APP-PSEN1 cells. (B5, 6) Two-tailed unpaired Student's t test. (B7) Two way (genotype and drug) ANOVA with repeated measures, n = 10 WT cells, 5 APP-PSEN1 cells. All immunohistochemical images presented represent a single optical section. The symbols represent the individual data points, the bars represent the means and the error bars the SEM. * = $P < 0.05$. Scale bars: 20 μm.

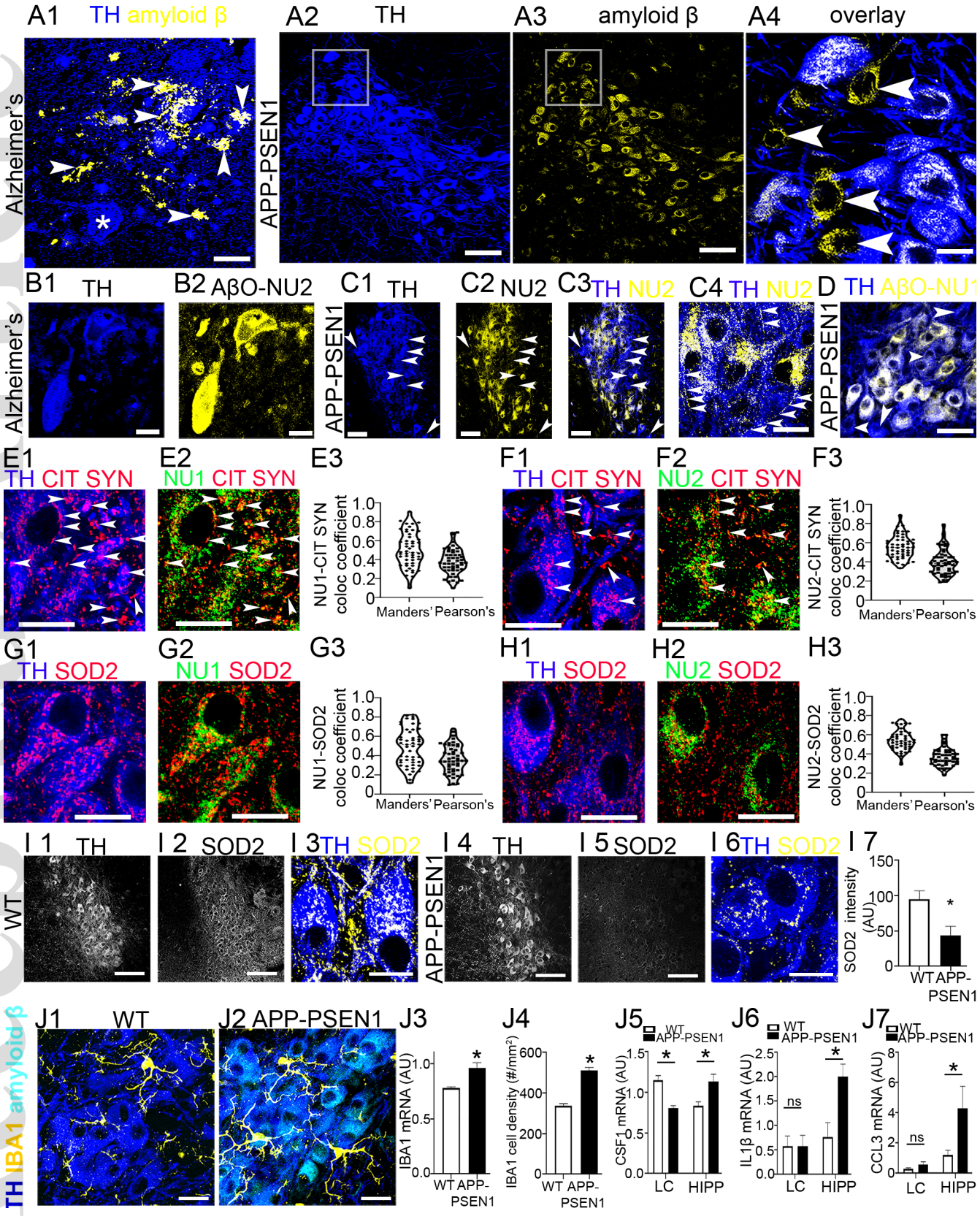

nan_12674_f1.tif

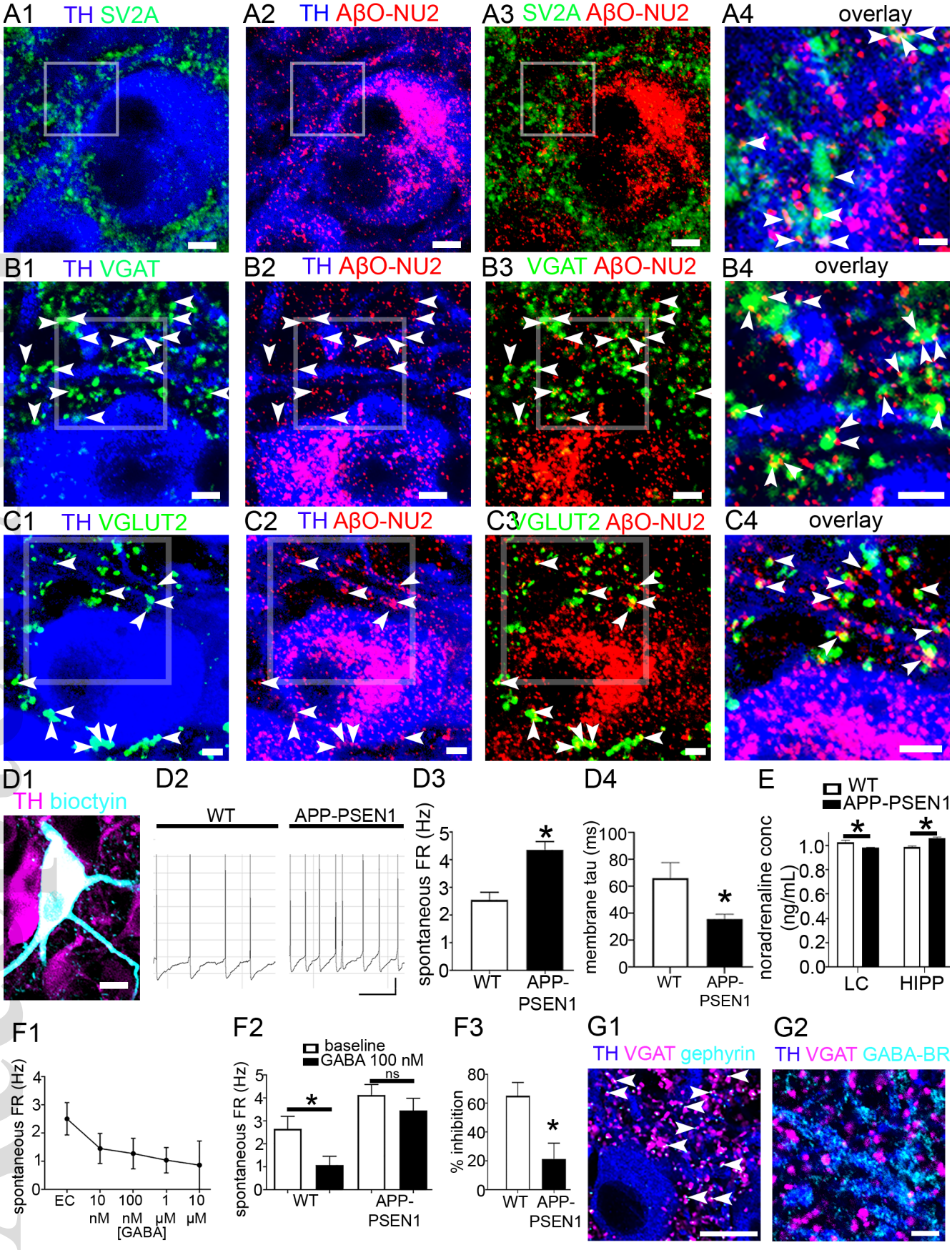

nan_12674_f2.tif

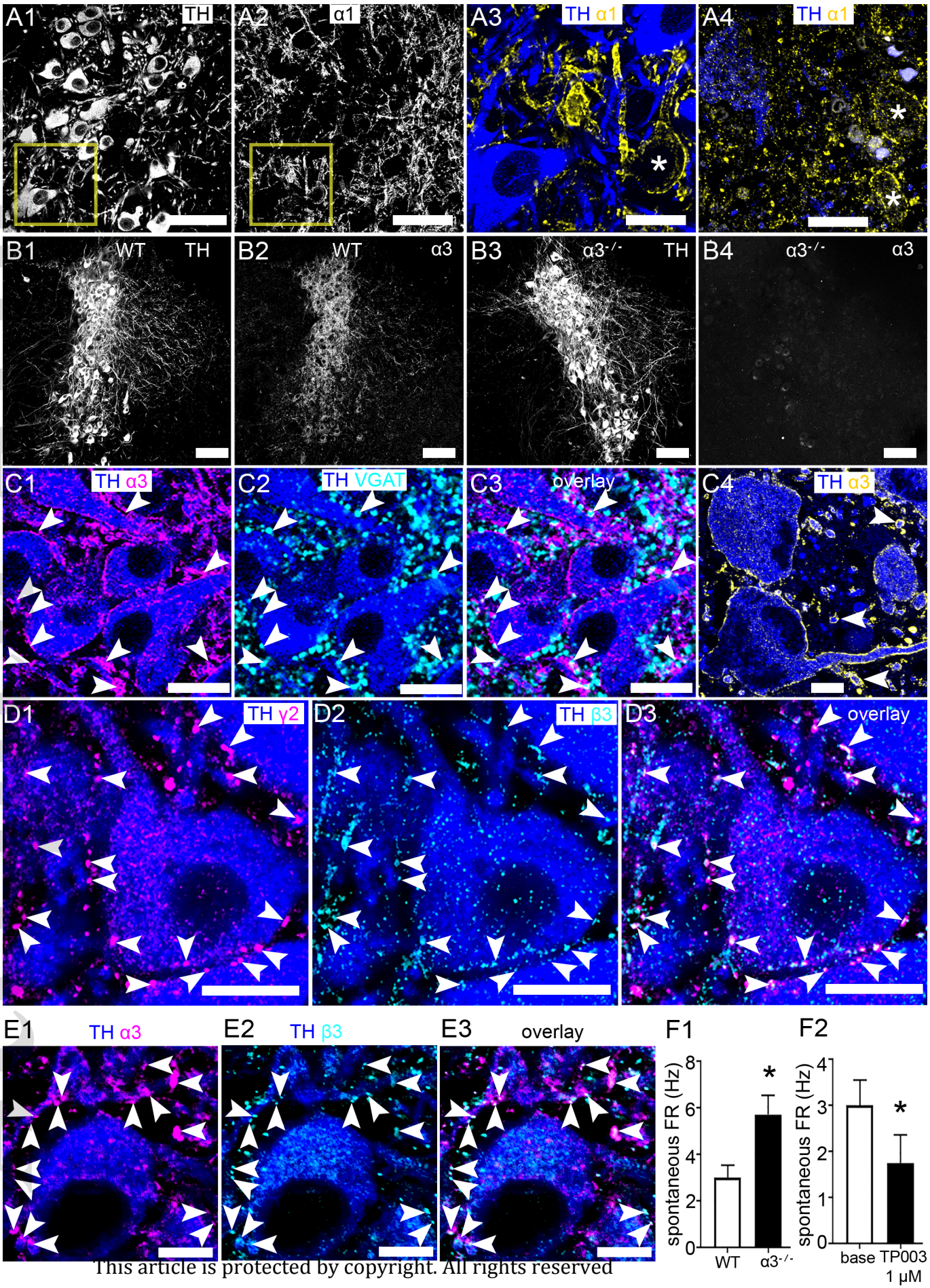

nan_12674_f3.tif

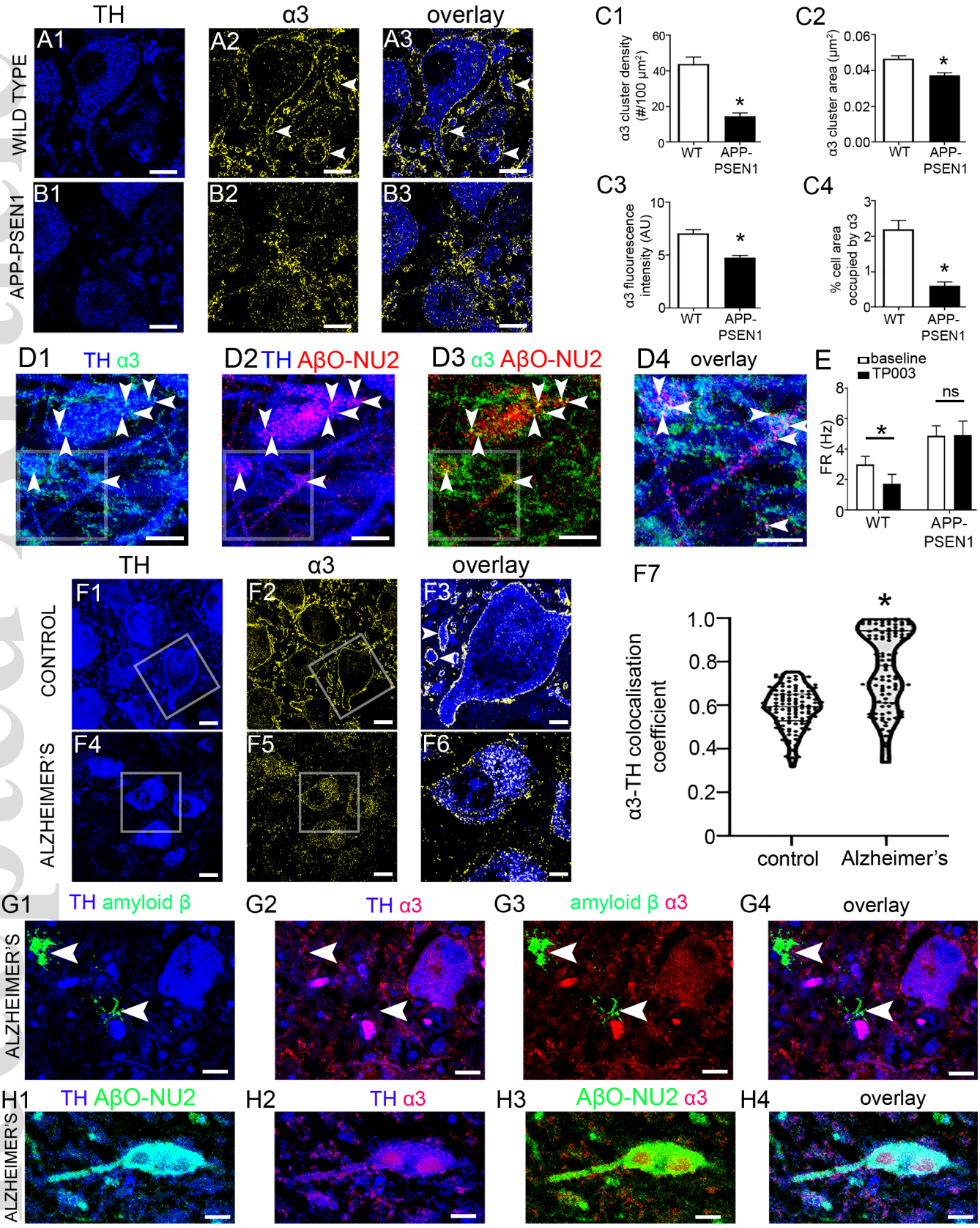

nan_12674_f4.tif

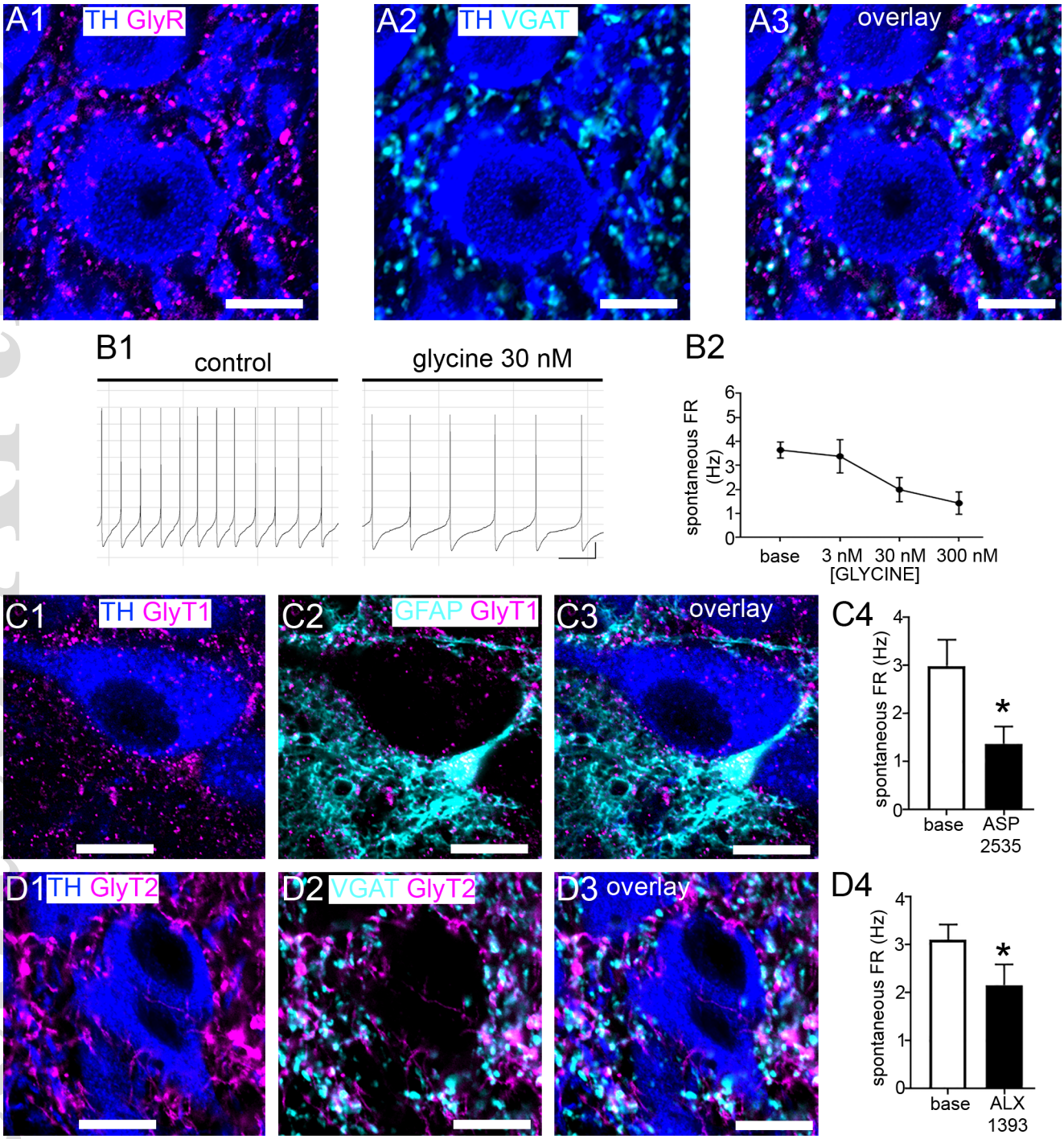

nan_12674_f5.tif

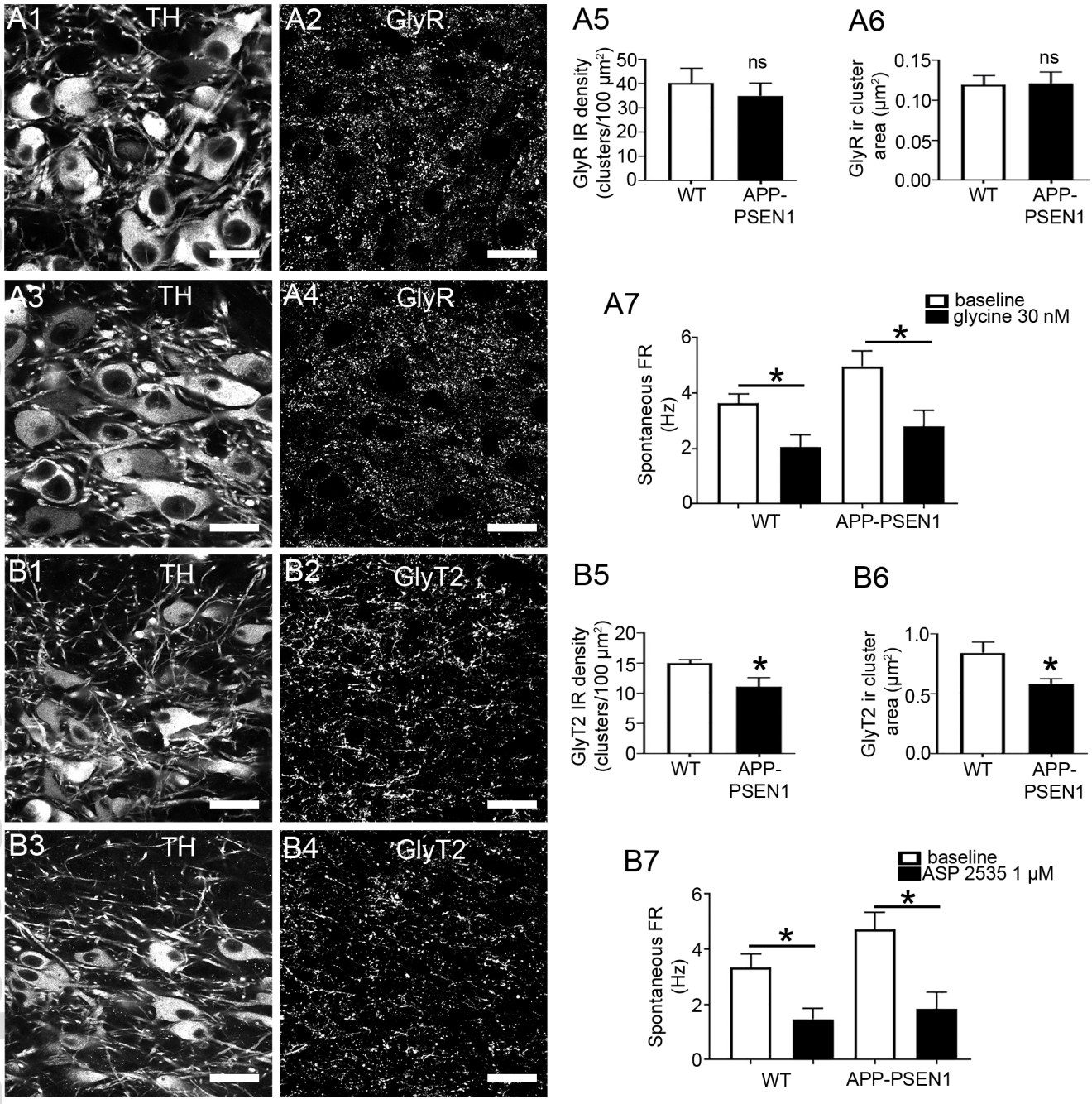

nan_12674_f6.tif